RESILIENT INFRASTRUCTURE

June 1–4, 2016

PROPOSED STRUT-AND-TIE MODEL FOR CONCRETE DEEP BEAMS REINFORCED WITH FRP BARS

Khaled Mohamed
Postdoctoral fellow, Université de Sherbrooke, Canada

Ahmed Sabry Farghaly
Postdoctoral fellow, Université de Sherbrooke, Canada

Brahim Benmokrane
Professor, Université de Sherbrooke, Canada
NSERC Research Chair in FRP Reinforcement for Concrete Infrastructure
Tier-1 Canada Research Chair in Advanced Composite Materials for Civil Structures

ABSTRACT

A compiled database of 53 tests of FRP-reinforced concrete deep beams with shear span–depth ratios of less than two was used to evaluate the strut-and-tie models (STM) provided in ACI 318 (2014), CSA S806 (2012), CEB-*fib* (1999), and JSCE (2007). All provisions were found to be inadequate in calculating the capacity of FRP-reinforced deep beams due to inherent shortcomings in each provision. Hence, a new STM-based procedure for FRP-reinforced deep beams was proposed. The new model incorporates the effect of shear span–depth ratio (a/d), concrete compressive strength (f_c'), and tensile strain in the adjoining tie (ε_1). The contribution of the web reinforcement on the strut efficiency factor was found to be insignificant. The new model was capable of predicting the ultimate capacity of the compiled FRP-reinforced concrete deep beams with satisfactory conservatism.

Keywords: Deep beams, Strut-and-Tie model, FRP rebars, Strut efficiency factor

1. INTRODUCTION

Reinforced-concrete deep beams are structural members with discontinuity regions (D-regions) in which the plane section does not remain plane; hence, the Bernoulli hypothesis and beam theory are not applicable (MacGregor 1997, Collins et al. 2008, Tuchscherer et al. 2011). Stresses in D-regions are dominated by shear, and shear stresses are resisted by arch-action mechanism. Accordingly, the design of D-regions must be treated differently from designing conventional sections (or slender beams). Researchers and code provisions have adopted the use of the strut-and-tie model to design and detail deep beams (ACI 318 2014, CSA S806 2012, CEB-*fib* 1999, JSCE 2007).

The strut-and-tie model (STM) is based on the lower-bound theorem, in which the stress applied on the elements of the STM should not exceed their maximum capacities, and the truss model shall be in equilibrium. When these conditions are met, the truss will exhibit the deformation capacity required by the lower-bound theorem to redistribute the internal stresses and form the arch action. Deep beams have varied applications as load-distribution elements such as transfer girders, pile caps, and bridge bents. When such elements are located in aggressive environments in which steel corrosion is a crucial factor, the use of fiber-reinforcement polymer (FRP) instead of steel bars is prudent. Therefore, various experimental investigations have been conducted to examine the behavior of FRP-reinforced deep beams (Kim et al. 2014, Latosh 2014, Andermatt and Lubell 2013, Farghaly and Benmokrane 2013, Nehdi et al. 2008). The test results show that an arch-action mechanism was able to form in FRP-reinforced deep beams. In addition, the deep beams tested exhibited sufficient deformation to redistribute the internal stresses as required by the STM (Andermatt and Lubell 2013, Farghaly and Benmokrane 2013). Only the Canadian CSA S806 (2012), however, recommended the use of the STM for FRP-reinforced deep beams.

The main objective of the current study was to assess the STM introduced in ACI 318 (2014), CEB-*fib* (1999), and JSCE (2007) for steel-reinforced deep beams and CSA S806 2012 for FRP-reinforced deep beams. The parameters affecting the strength of the deep beams were identified, and the tendency of each parameter was individually assessed using the data on experimentally tested deep beams in the literature. Finally, a new STM-based procedure was proposed for the design and detailing of FRP-reinforced deep beams.

To achieve the objective of this paper, the authors compiled a database of 53 experimental tests for FRP-reinforced deep beams from the literature (Mohamed 2015, Kim et al. 2014, Latosh 2014, Andermatt and Lubell 2013, Farghaly and Benmokrane 2013, Nehdi et al. 2008). Table 1 presents details of the deep beams included in the database. Specimens described by the authors as having a failure mode other than shear (flexural and/or anchorage failures) were excluded. In addition, significantly smaller specimens (with effective depths of less than 200 mm) were also excluded, as it is difficult to present dimensional accuracy in reinforcement details, concrete geometry, and testing setup using highly scaled specimens comparing to deep beams in reality. An effective depth limit of 200 mm could be reasonable, however, more investigations are needed to identify the size effect on the RC deep beams. The deep beams included in the assessment had a/d values ranging from 0.83 to 2.10, concrete strengths ranging from 26.1 to 68.5 MPa, various combinations of web reinforcement, and different types of FRP bars (AFRP, CFRP, and GFRP).

Table 1: Details of database specimens

Specimen ID	b mm	d mm	a/d	l_{b1} mm	l_{b2} mm	f_c' MPa	Type of FRP Bar	A_{frp} mm²	E_{frp} GPa	ρ_v %	ρ_h %	P_{exp} kN	ACI 318 P_{exp}/P_{pred}	CSA S806 P_{exp}/P_{pred}	CEB-*fib* 1999 P_{exp}/P_{prop}	JSCE 2007 P_{exp}/P_{prop}	Proposed Model P_{exp}/P_{prop}
CF-d-250[1]	150	250	1.35	50	50	41.7	CFRP	506.3	134	-	-	298.1	0.79	2.24	1.76	1.33	0.77
CF-d-350[1]	150	350	1.21	50	50	37.6	CFRP	635.3	134	-	-	468.2	1.31	3.20	2.92	2.21	1.00
F-d-250[1]	150	250	1.39	50	50	42.0	GFRP	521.3	40.8	-	-	243.1	0.64	2.74	1.42	1.07	0.80
F-d-350[1]	150	350	1.25	50	50	48	GFRP	656.3	40.8	-	-	422.5	0.93	3.69	2.06	1.56	1.13
A1N[1]	310	257	1.07	100	100	40.2	GFRP	1188	41.1	-	-	814	1.00	1.86	1.00	0.78	1.08
A2N[2]	310	261	1.44	100	100	45.4	GFRP	1188	41.1	-	-	472	0.66	1.68	0.66	0.50	1.15
A3N[2]	310	261	2.02	100	100	41.3	GFRP	1188	41.1	-	-	244	0.55	1.89	0.55	0.41	1.44
A4N[2]	310	261	2.02	100	100	64.6	GFRP	1188	41.1	-	-	192	0.28	1.13	0.28	0.20	0.99
B1N[2]	300	503	1.08	200	200	40.5	GFRP	2576	37.9	-	-	1274	0.81	1.50	0.81	0.63	0.88
B2N[2]	300	501	1.48	200	200	39.9	GFRP	2576	37.9	-	-	800	0.68	1.66	0.68	0.52	1.10
B3N[2]	300	502	2.07	200	200	41.2	GFRP	2576	37.9	-	-	432	0.53	1.82	0.53	0.39	1.40
B4N[2]	300	496	1.48	200	200	40.7	GFRP	3168	41.1	-	-	830	0.69	1.53	0.69	0.53	1.04
B5N[2]	300	497	1.48	200	200	66.4	GFRP	3168	41.1	-	-	1062	0.54	1.44	0.54	0.41	1.16
B6N[2]	300	505	2.06	200	200	68.5	GFRP	2576	37.9	-	-	376	0.27	1.14	0.27	0.20	1.03
C1N[2]	301	889	1.10	330	330	51.6	GFRP	4224	42.3	-	-	2270	0.68	1.36	0.68	0.53	0.87
C2N[2]	304	891	1.49	330	330	50.7	GFRP	4224	42.3	-	-	1324	0.53	1.38	0.53	0.40	1.00
G6#8[3]	300	1097	1.13	232	130	49.3	GFRP	2280	47.6	-	-	1477	1.17	1.96	1.17	0.90	1.26
G8#8[3]	300	1088	1.13	232	130	49.3	GFRP	4054	51.9	-	-	1906	1.51	1.97	1.51	1.17	1.30
C12#3[3]	300	1111	1.13	232	130	38.7	GFRP	856	120	-	-	1191	1.19	1.83	1.19	0.92	1.06
C12#4[3]	300	1106	1.13	232	130	38.7	GFRP	1520	144	-	-	1601	1.60	1.85	1.60	1.24	1.07
A3D9M-1.4[4]	200	250	1.40	100	100	26.1	AFRP	190	80.70	-	-	136.1	0.50	1.32	0.50	0.38	1.07
A3D9M-1.7[4]	200	250	1.70	100	100	26.1	AFRP	190	80.70	-	-	98.98	0.45	1.42	0.45	0.34	1.23
A3D9M-2.1[4]	200	250	2.10	100	100	26.1	AFRP	190	80.70	-	-	88.00	0.52	2.03	0.52	0.38	1.26
A4D9M-1.7[4]	200	250	1.70	100	100	26.1	AFRP	255	80.70	-	-	121.0	0.55	1.55	0.55	0.41	0.91
A5D9M-1.7[4]	200	250	1.70	100	100	26.1	AFRP	320	80.70	-	-	134.0	0.61	1.57	0.61	0.45	1.40
A5D9L-1.7[4]	200	310	1.70	100	100	26.1	AFRP	255	80.70	-	-	134.3	0.59	1.69	0.59	0.44	1.48
C3D9M-1.4[4]	200	250	1.40	100	100	26.1	CFRP	190	120.2	-	-	169.3	0.62	1.40	0.62	0.48	1.15
C3D9M-1.7[4]	200	250	1.70	100	100	26.1	CFRP	190	120.2	-	-	106.5	0.48	1.31	0.48	0.36	1.16
C3D9M-2.1[4]	200	250	2.10	100	100	26.1	CFRP	190	120.2	-	-	52.60	0.31	1.04	0.31	0.23	1.00
C4D9M-1.7[4]	200	250	1.70	100	100	26.1	CFRP	255	120.2	-	-	96.1	0.43	1.06	0.43	0.33	0.95
C5D9M-1.7[4]	200	250	1.70	100	100	26.1	CFRP	320	120.2	-	-	151.4	0.68	1.54	0.68	0.51	1.39

Table 1: Details of database specimens (cont'd.)

Specimen ID	b (mm)	d (mm)	a/d	l_{b1} (mm)	l_{b2} (mm)	f_c' MPa	Type of FRP Bar	A_{frp} (mm²)	E_{frp} (GPa)	ρ_v (%)	ρ_h (%)	P_{exp} (kN)	ACI 318 P_{exp}/P_{pred}	CSA S806 P_{exp}/P_{pred}	CEB-fib 1999 P_{exp}/P_{prop}	JSCE 2007 P_{exp}/P_{prop}	Proposed Model P_{exp}/P_{prop}
C5D9L-1.7[4]	200	310	1.70	100	100	26.1	CFRP	255	120.2	-	-	145.4	0.64	1.14	0.39	0.29	1.01
A1/100[5]	230	621	1.00	180	180	49.8	GFRP	1710	47.6	0.14	-	560.3	0.57	1.36	0.78	0.37	1.24
A1/75[5]	230	621	1.00	180	180	52.2	GFRP	1710	47.6	0.10	-	552.4	0.53	1.30	0.73	0.35	1.20
A1/50[5]	230	621	1.00	180	180	52.5	GFRP	1710	47.6	0.06	-	493.7	0.47	1.16	0.65	0.31	1.08
A1/00[5]	230	621	1.00	180	180	52.7	GFRP	1710	47.6	-	-	416.9	0.55	0.98	0.55	0.43	0.91
B1.5/100[5]	230	447	1.50	180	180	51.8	GFRP	1235	47.0	0.15	-	322.4	0.47	1.80	0.62	0.24	1.95
C2/100[5]	230	328	2.00	180	180	50.8	GFRP	760.2	46.3	0.16	-	125.9	0.28	1.63	0.36	0.15	1.53
C2/75[5]	230	328	2.00	180	180	51.0	GFRP	760.2	46.3	0.10	-	98.7	0.22	1.27	0.28	0.12	1.20
C2/50[5]	230	328	2.00	180	180	51.3	GFRP	760.2	46.3	0.06	-	102.7	0.23	1.32	0.29	0.13	1.24
C2/00[5]	230	328	2.00	180	180	51.3	GFRP	760.2	46.3	-	-	93.5	0.26	1.20	0.26	0.20	1.13
G1.47[6]	300	1088	1.47	232	203	38.7	GFRP	4054	66.4	-	-	1849	1.50	2.48	1.50	1.12	1.66
G1.47H[6]	300	1088	1.47	232	203	45.4	GFRP	4054	66.4	-	0.68	1695	0.78	2.05	1.17	0.45	1.48
G1.47V[6]	300	1088	1.47	232	203	45.4	GFRP	4054	66.4	0.42	-	2650	1.22	3.21	1.83	0.70	2.31
G1.13[6]	300	1088	1.13	232	203	37	GFRP	4054	66.4	-	-	2687	1.84	2.34	1.84	1.43	1.36
G1.13H[6]	300	1088	1.13	232	203	44.6	GFRP	4054	66.4	-	0.68	2533	1.01	1.96	1.44	0.64	1.24
G1.13V[6]	300	1088	1.13	232	203	44.6	GFRP	4054	66.4	0.42	-	3236	1.29	2.51	1.84	0.82	1.59
G1.13VH[6]	300	1088	1.13	232	203	37	GFRP	4054	66.4	0.42	0.68	2904	1.39	2.53	1.99	0.88	1.47
G0.83[6]	300	1088	0.83	232	203	38.7	GFRP	4054	66.4	-	-	3000	1.62	1.59	1.62	1.30	0.80
G0.83H[6]	300	1088	0.83	232	203	43.6	GFRP	4054	66.4	-	0.68	3166	1.11	1.56	1.51	0.78	0.82
G0.83V[6]	300	1088	0.83	232	203	43.6	GFRP	4054	66.4	0.42	-	3387	1.19	1.67	1.62	0.83	0.88
SG1.13[6]	300	1088	1.13	232	203	43.1	GFRP	3928	66.0	-	-	2928	1.72	2.35	1.00	1.33	1.46
SG1.13VH[6]	300	1088	1.13	232	203	43.1	GFRP	3928	66.0	0.42	0.68	3110	1.28	2.50	1.07	0.81	1.55
Mean value													0.80	1.77	0.94	0.64	1.20
CoV													54%	33%	64%	65%	24%

b is the beam width; d is the effective depth; a/d is the shear span-depth ratio; l_{b1} and l_{b2} are the loading- and support-plate widths, respectively; ρ_v is the vertical web-reinforcement ratio; ρ_h is the horizontal web-reinforcement ratio; P_{exp} is the ultimate load at failure recorded during testing; P_{pred} is the predicted load. References: [1]Nehdi et al. (2008), [2]Andermatt and Lubell (2013), [3]Farghaly and Benmokrane (2013), [4]Kim et al. (2014), [5]Latosh (2014), [6]Mohamed (2015).
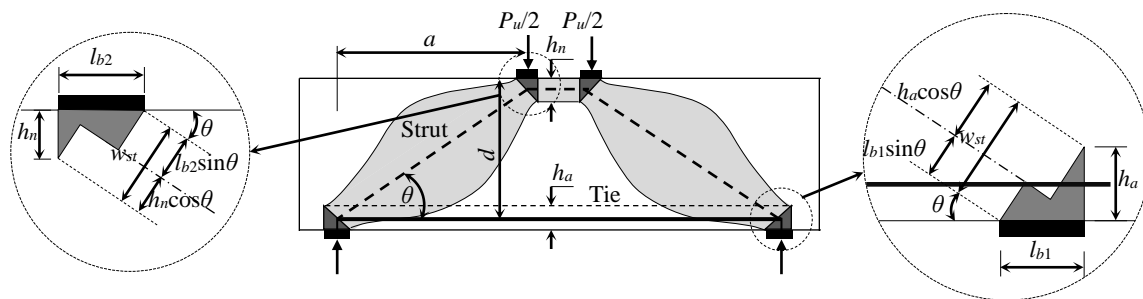
2. STRUT-AND-TIE MODEL

Figure 1: Details of a one-panel strut-and-tie model

Researchers and practitioners consider the STM to be the most convenient tool for D-region design when the conventional plane-bending theory does not hold. The use of the STM allows for easy visualization of force flow and reduces complex states of stress within a D-region in a reinforced-concrete member into a truss comprised of simple, uniaxial stress paths. Each uniaxial stress path is considered an STM member (Figure 1). Members of the STM subjected to tensile stresses are called ties and represent where reinforcement should be placed. STM members

subjected to compression are called struts. The intersections of truss members are called nodes. Nodes are named based on the bounded elements. For instance, nodal zones are called CCC, CCT, or CTT nodes, respectively, depending on the number of struts bounding them (three, two, or one).

To avoid tie failure, codes and provisions require a sufficient amount of longitudinal reinforcement to be placed as a tie. Generally, the area of the longitudinal reinforcement should be more than or equal to $P_u / \tan \theta . f_s$, where P_u is the maximum applied load and f_s is the allowable tensile strength (yield strength for steel and ultimate strength for FRP bars). In our database, no failure in the FRP longitudinal reinforcement was observed as the measured strains in the longitudinal FRP-reinforcement were below 60% of ultimate tensile strength of the bars (f_{frpu}). Hence, this value is recommended ($f_{frp} \leq 0.6 f_{frpu}$) to achieve an adequate amount of FRP longitudinal reinforcement.

To avoid crushing of the concrete elements, most researchers and code specifications limit the compressive stress of the concrete (f_{ce}) as the product of the concrete compressive strength (f_c') and an efficiency factor (β) as follows:

[1] $\qquad f_{ce} = \beta . f_c'$

As can be seen from Eq. 1, β can be defined as the ratio of the stress in the concrete element to the concrete's compressive strength. Generally, the procedure was to account for all the parameters affecting the concrete's compressive strength (such as the reinforcement details, stress and strain conditions, and concrete softening) in a single factor referred to as β. While various studies have been conducted to assess the value of β for steel-reinforced deep beams (Reineck and Todisco 2014, Brown and Bayrak 2008), its value differs (see Table 2) for struts and nodes designed according to ACI 318 (2014), CSA S806 (2012), CEB-*fib* (1999), and JSCE (2007).

Once f_{ce} has been calculated for concrete elements (struts and nodes), the maximum resisting force of the element can be calculated by multiplying f_{ce} by the area of the element (A_c), as shown in Figure 1. Calculating the depth of the top horizontal strut (h_n) and thus the diagonal strut angle (θ), is an iterative process required to select the critical admissible solution and the maximum predicted shear strength based on the lower-bound theorem.

Table 2: Efficiency factors according to code provisions

Element	Efficiency Factor (β)			
	ACI 318 (2014)	CSA S806 (2012)	CEB-*fib* (1999)	JSCE (2007)
Struts without web reinforcement	0.85×0.60	$\dfrac{1}{0.8+170\varepsilon_1} \leq 0.85$ $\varepsilon_1 = \varepsilon_F + (\varepsilon_F + 0.002)\cot^2 \theta$	0.85×0.60*	0.60
Struts with web reinforcement	0.85×0.75	$\dfrac{1}{0.8+170\varepsilon_1} \leq 0.85$ $\varepsilon_1 = \varepsilon_F + (\varepsilon_F + 0.002)\cot^2 \theta$	0.85×0.60*	0.80
CCC node	0.85×1.00	0.85	0.85×0.60*	1.00
CCT node	0.85×0.80	0.75	0.85×0.60*	1.00
CTT node	0.85×0.60	0.65	0.85×0.60*	1.00

where θ is the angle between the strut and tie, ε_F is the tensile strains in the tie bars adjacent to the compressive strut, and f_c' is the concrete compressive strength in MPa.
* β in according to CEB-*fib* (1999) should be less than $0.85(1-f_c'/250)$

3. ASSESSMENT OF CURRENT DESIGN PROVISIONS

The efficiency-factor equations in Table 2 were used to calculate the capacities of the FRP-reinforced deep beams in our database. Table 1 provides the predicted capacities according to ACI 318 (2014), CSA S806 (2012), CEB-*fib* (1999), and JSCE (2007). Figure 2 shows the comparison between the experimental results and the predicted

capacity for each code provision. The results of the predicted capacities for all of the codes were scattered and not adequately predicted, revealing that each provision has different deficiencies.
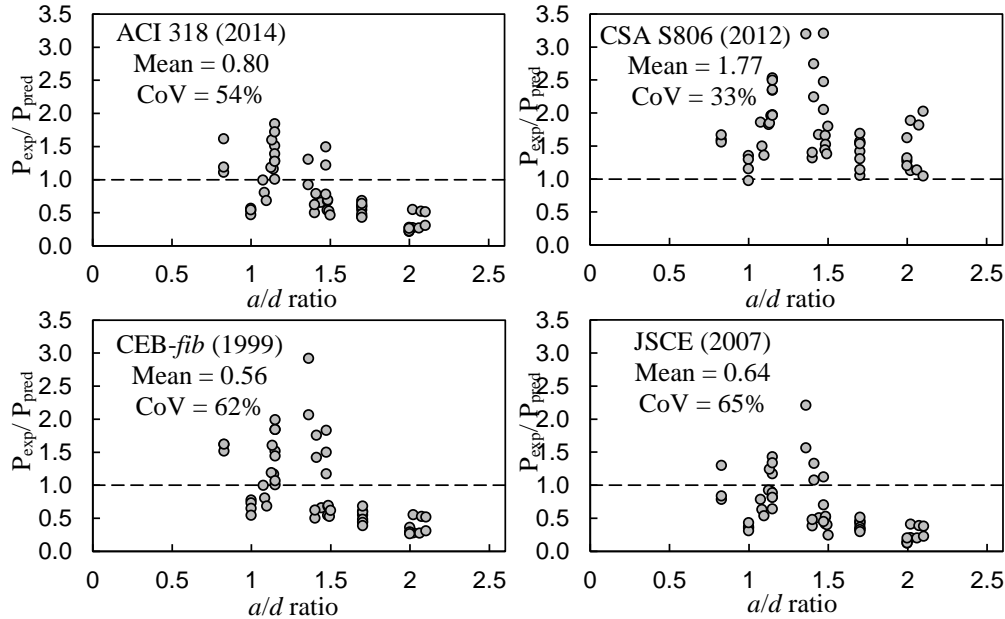

Figure 2: Comparison of experimental and predicted capacity using the STM in code provisions

The STM in the ACI provision produced unsafe and arbitrary estimations for the capacities of the deep beams in our database, with a mean experimental-to-predicted value of 0.80 and coefficient of variation (CoV) of 54%. These unsafe estimations have also been reported for steel-reinforced deep beams without web reinforcement (Reineck and Todisco 2014, Tuchscherer et al. 2014), but with lower levels of safety in FRP-reinforced deep beams. This could be attributed to the fact that the efficiency factor recommended in ACI 318 (2014) accounts only for the presence of web reinforcement (see Table 2), and neglects other major parameters, such as concrete softening, f_c', and a/d ratio. Additionally, the effect of web reinforcement on the strength of the FRP-reinforced deep beams was found to be insignificant (Mohamed et al. 2014).

The STM in CSA S806 (2012) yielded safe yet conservative estimations for the deep beams in our database. The level of conservatism—with a mean experimental-to-predicted value of 1.77 and CoV of 32%—could lead to uneconomical design for FRP-reinforced deep beams. As shown in Table 2, the STM in CSA S806 (2012) explicitly accounts for the concrete softening coefficient in the diagonal strut by calculating the strut efficiency factor as a factor of the strains in the longitudinal reinforcement (ε_F). This implicitly accounts for the shear span–depth ratio by taking into account the angle between the strut and tie (θ), and does not account for the effect of the concrete compressive strength (f_c').

The calculation of the strut efficiency factor in CSA S806 (2012) is the same as that for the design of steel-reinforced deep beams in CSA A23.3 (2014). It is expected, however, that the softening coefficient of FRP-reinforced members is higher than that of steel-reinforced members due to FRP bars having higher tensile strain than steel bars. In steel-reinforced deep beams, the longitudinal steel bars should not yield, thus strains in the longitudinal steel bars would be lower than 0.002. On the other hand, FRP bars have low elastic moduli and higher strains compared to steel bars. These higher strains induce higher strains in the concrete surrounding the FRP bars, which could lead to higher concrete softening in FRP-reinforced members. This could explain the underestimated capacity produced by the STM in CSA S806 (2012).

The strut efficiency factor (β) recommended by CEB-*fib* (1999) takes into consideration the effect of the concrete compressive strength (f_c'), but for $f_c' \geq 100$ MPa. Therefore, the f_c' had no impact on the strut efficiency factors for the deep beams in our database, and a constant value of β equal to 0.85×0.6 was taken instead. This led to the unsafe scattered estimation of the capacity prediction according to the STM in CEB-*fib* (1999), with a mean experimental-to-predicted value of 0.94 and CoV of 64%.

Similar to ACI 318 (2014), JSCE (2007) stipulates constant values for the strut efficiency factor depending only on the presence of web reinforcement. JSCE (2007) was also unable to satisfactorily predict the capacity of the FRP-reinforced deep beams, with a mean experimental-to-predicted value of 0.70 and CoV of 61%. As in the case of the ACI code, these unsafe and arbitrary results could be attributed to the negligence of the concrete softening coefficient, f_c', and a/d ratio. Nevertheless, the lower level of safety provided by JSCE (2007) in comparison to the ACI code could be attributed to the higher value of strut efficiency factor recommended by JSCE (2007).

4. PROPOSED STRUT-AND-TIE MODEL

The selected database was used to identify the parameters affecting the strut efficiency factor of the FRP-reinforced deep beams. Figure 3 provides the individual effect of each parameter influencing the strut efficiency factor. These parameters were found to be the strain in the longitudinal reinforcement (ε_1), the concrete compressive strength (f_c'), the shear span-depth ratio (a/d), and the web reinforcement (ρ_w). The trend of each parameter affecting the strut efficiency and the curve best-fitting equation are also presented in Figure 3.
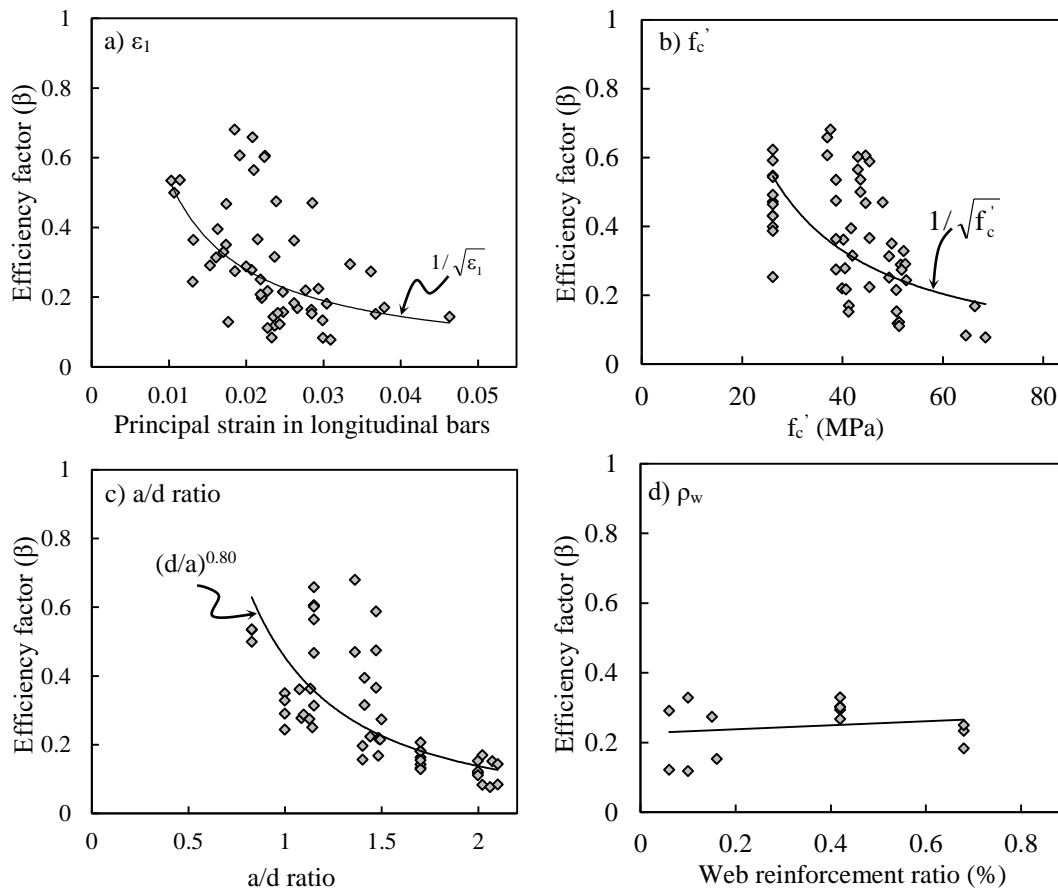

Figure 3: Influence of parameters affecting the strut efficiency factor

Figure 3 (a) shows the effect of the longitudinal-bar strain on strut efficiency, as increasing the tensile–tie strains decreases strut efficiency. Farghaly and Benmokrane (2013) illustrated that reducing the longitudinal reinforcement ratios—while maintaining all other pertinent variables constant—increased the measured tensile-tie strains, leading to a noticeable enhancement in the diagonal-strut strength, and thus the overall capacity of the specimens. This could be explained by increased tensile strains in the ties exposing the adjacent concrete strut to tensile stresses, thereby reducing concrete strength due to concrete softening (Vecchio and Collins 1993, Zhang and Hsu 1998). Concrete softening is commonly referred to the reduction of concrete strength and stiffness due to the presence of high tensile

strains in the direction normal to the compression. As discussed previously, concrete softening in steel-reinforced deep beams could be relatively lower than that in FRP-reinforced deep beams, due to the relatively higher tensile strains exhibited in FRP bars at ultimate load comparing to steel bars prior yielding.

It is worth mentioning that concrete softening in compression is a function of the principal tensile strain (ε_1) rather than direct strains in the longitudinal reinforcement (Vecchio and Collins 1986). Therefore, the efficiency factor in Figure 3(a) was related to ε_1, where ε_1 can be calculated as suggested in CSA S806 (2012) as follows:

[2] $\qquad \varepsilon_1 = \varepsilon_F + (\varepsilon_F + 0.002)\cot^2\theta$

Figure 3 (b) shows the negative effect of f_c' on the efficiency factor of the concrete strut. This effect was explained by Andermatt and Lubell (2013) by testing identical specimens with different f_c'. Andermatt and Lubell (2013) found that the more brittle nature of the high-strength concrete limited the deformation of the deep beams, and reduced the diagonal strut's efficiency. Many researchers (Kim et al. 2014, Andermatt and Lubell 2013) have reported on the effect of a/d ratio on the strength of deep beams, since increasing the a/d ratio decreases strut strength, as shown in Figure 3(c).

Mohamed et al. (2014) studied the effect of web reinforcement on the strength of FRP-reinforced deep beams by using different web-reinforcement configurations (including horizontal only, vertical only, and vertical and horizontal). Generally, based on the limited available data for FRP-reinforced deep beams (total of 10 specimens), the presence of web reinforcement had no significant effect on the strut efficiency factor, as shown in Figure 3(d). This was also observed in the steel-reinforced deep beams tested by Birrcher et al. (2013).

Based on the results shown in Figure 3, and performing least-squares regression to identify the effect of each parameter affecting the strength of the strut, the following diagonal-strut efficiency factor is proposed:

[3] $\qquad \beta = 0.5\dfrac{1}{\sqrt{f_c'}}\dfrac{1}{(a/d)^{0.8}}\dfrac{1}{\sqrt{\varepsilon_1}}$ where ε_1 is given in Eq. 2.

Figure 4 shows the comparison between the experimental results and the capacity prediction using the proposed model (Eq. 3) for the deep beams in our database. The proposed model produced safe capacity estimates with a mean experimental-to-predicted value of 1.20 and CoV of 24%. Additionally, the predicted capacity was governed by diagonal-strut failure, which is consistent with the experimental results. Nevertheless, the model underestimated the capacity of some specimens, most of which were found to have vertical web reinforcement. Therefore, it is suggested that the vertical bars may develop a more refined load-transfer mechanism than that assumed in the one-panel truss mechanism shown in Figure 1. Brown and Bayrak (2008) indicated that, for steel-reinforced deep beams, increasing the amount of vertical web reinforcement can shift portions of the load to a two-panel mechanism. Additional research is needed to investigate such a mechanism in FRP-reinforced deep beams.
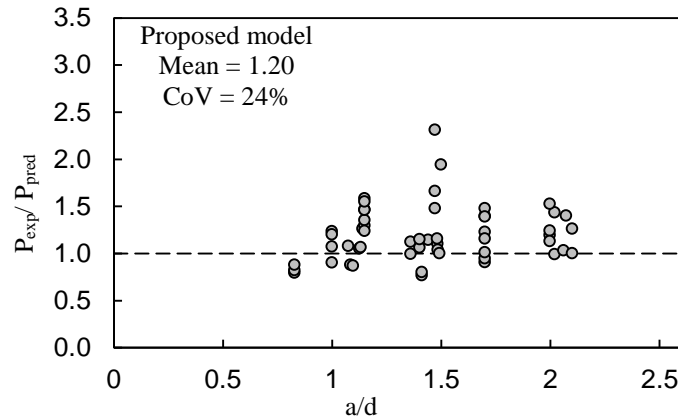

Figure 4: Predicted capacity using the proposed model

5. CONCLUSIONS

In our study, a database of 53 FRP-reinforced deep beams was compiled from the literature to assess the adequacy of the current STMs in ACI 318 (2014), CSA S806 (2012), CEB-*fib* (1999), and JSCE (2007), and to propose a new strut-and-tie-based model. The following conclusions were drawn:

1. The STMs in ACI 318 (2014), CEB-*fib* (1999), and JSCE (2007) use constant values for calculating strut efficiency, which led to unsafe estimations of the capacities of the deep beams in our database with mean experimental-to-predicted values of 0.80, 0.56, and 0.64, respectively.
2. The STM in CSA S806 (2012) produced conservative yet underestimated predictions of the capacities of the deep beams in our database, which could lead to uneconomical designs of FRP-reinforced deep beams.
3. The strut efficiency factor is negatively affected by increased strains in the longitudinal reinforcement (ε_1), the shear span-depth ratio (a/d), and the concrete compressive strength (f_c').
4. The limited data available for FRP-reinforced deep beams showed that the web-reinforcement ratio (ρ_w) had an insignificant effect on the diagonal-strut strength. More experimental investigations are needed to verify this effect.

The new strut efficiency factor was proposed based on the parameters affecting the strut strength (Eq. 3). The proposed model was verified against the compiled database and produced safe capacity estimates with an acceptable level of conservatism. The compiled database had a/d values ranging from 0.83 to 2.10, concrete strengths ranging from 26.1 to 68.5 MPa, various combinations of web reinforcement, and different types of FRP bars (AFRP, CFRP, and GFRP). More experimental investigations are needed to further verify the proposal model.

REFERENCES

ACI Committee 318 2014. Building Code Requirements for Structural Concrete and Commentary (ACI 318-14). *American Concrete Institute*, Farmington Hills, MI, USA, 473 pp.

Andermatt, M. F. and Lubell A. S. 2013. Behavior of Concrete Deep Beams Reinforced with Internal Fiber-Reinforced Polymer—Experimental Study. *ACI Structural Journal*, 110 (4): 585-594.

Birrcher, D. B., Tuchscherer, R. G., Huizinga, M. and Bayrak, O. 2013. Minimum Web Reinforcement in Deep Beams, *ACI Structural Journal*, 110 (2): 297-306.

Brown, M. D. and Bayrak, O. 2008. Design of Deep Beams Using Strut-and-Tie Models-Part I: Evaluating U.S. Provisions, *ACI Structural Journal*, 105 (4): 395-404.

CEB-*fib* Fédération Internationale du Béton Structural Concrete 1999. Textbook on Behaviour, Design, and Performance. Volume 1 (bulletin 1), *International Federation for Structural Concrete*, Lausanne, Switzerland.

Collins, M. P., Bentz, E. C. and Sherwood, E. G. 2008. Where is Shear Reinforcement Required? Review of Research Results and Design Procedures. *ACI Structural Journal*, 105(5): 590-600.

CSA A23.3 2014. Design of Concrete Structures Standard. *Canadian Standards Association*, Mississauga, Ontario, Canada, 240 pp.

CSA S806 2012. Design and Construction of Building Components with Fiber-Reinforced Polymers. *Canadian Standards Association*, Mississauga, Ontario, Canada, 208 pp.

Farghaly, A. S. and Benmokrane, B. 2013. Shear Behavior of FRP-Reinforced Concrete Deep Beams without Web Reinforcement." *ASCE Journal of Composites for Constructions*, 17 (6): 04013015.1-10.

Japan Society of Civil Engineers (JSCE) 1997. Recommendations for Design and Construction of Concrete Structures Using Continuous Fiber Reinforced Materials, *Research Committee on Continuous Fibre Reinforced Materials*, editor: A. Machida, Tokyo, Japan.

Kim, D., Lee, J. and Lee, Y-H. 2014. Effectiveness Factor of Strut-and-Tie Models for Concrete Deep Beams Reinforced with FRP Rebars. *Composites Engineering: Part B*, 56 (2014): 117-125.

Latosh, F. A. 2014. Structural Behaviour of Conventional and FRP-Reinforced Concrete Deep Beams, Ph.D. Thesis, Department of Building, Civil, and Environmental Engineering, *Concordia University*, Montréal, Québec, Canada.

MacGregor, J. G. 1997. Reinforced Concrete, Mechanics and Design, 3rd Edition, Prentice Hall, New Jersey, USA.

Mohamed, K., Farghaly, A. S. and Benmokrane, B. 2014. Effect of Web Reinforcement in FRP-Reinforced Deep Beams. *7th International Conference in FRP Composites in Civil Engineering* (CICE2014), Vancouver, BC, Canada, 6 p.

Mohamed, K., 2015. Performance and Strut Efficiency Factor of Concrete Deep Beams Reinforced with GFRP Bars, Ph.D. Thesis, *Université de Sherbrooke*, Sherbrooke, Québec, Canada.

Nehdi, M., Omeman, Z. and El-Chabib, H. 2008. Optimal Efficiency Factor in Strut-and-Tie Model for FRP-Reinforced Concrete Short Beams with (1.5 < a/d < 2.5), *Materials and Structures*, 41 (10): 1713-1727.

Reineck, K. and Todisco, L. 2014. Database of Shear Tests for Non-Slender Reinforced Concrete Beams without Stirrups. *ACI Structural Journal*, 111 (6): 1363-1372.

Tuchscherer, R., Birrcher, D., Huizinga, M. and Bayrak, O. 2011. Distribution of Stirrups across Web of Deep Beams, *ACI Structure Journal*, 108 (1): 108-115.

Tuchscherer, R. G., Birrcher, D. B., Williams, C. S., Deschenes, D. J. and Bayrak, O. 2014. Evaluation of Existing Strut-and-Tie Methods and Recommended Improvements. *ACI Structural Journal*, 111 (6): 1451-1460.

Vecchio, F. J. and Collins, M. P. 1993. Compression Response of Cracked Reinforced Concrete, *ASCE Journal of Structural Engineering*, 119 (12): 3590-3610.

Vecchio, F. J. and Collins, M. P. 1986. Modified Compression Field Theory for Reinforced Concrete Elements Subjected to Shear, *ACI Structural Journal*, 83 (2): 219-231.

Zhang, L. X. and Hsu, T. T. C. 1998. Behavior and Analysis of 100 MPa Concrete Membrane Elements, *Journal of Structural Engineering*, 124 (1): 24-34.